# Spin coated chitin films for biosensors and its analysis are depended on chitin-surface interactions

Marco G. Casteleijn[#1], Dominique Richardson[1], Petteri Parkkila[1], Niko Granqvist[2], Arto Urtti[1,3], Tapani Viitala[1].

1) Drug Research Program, Division of Pharmaceutical Biosciences, Faculty of Pharmacy, University of Helsinki, Finland; 2) BioNavis Ltd., Tampere, Finland, 3) School of Pharmacy, Faculty of Health Sciences, University of Eastern Finland, Kuopio, Finland

# Corresponding author: Marco Casteleijn, Division of Pharmaceutical biosciences and the Drug Research Program, University of Helsinki, Viikinkaari 5 E, 00014 University of Helsinki, FINLAND. marco.casteleijn@helsinki.fi

**Keywords:** Chitin, Surface Plasmon Resonance, Chitin Binding Domain, Split-Inteins, Biosensor, Layer Modeling.

## Abstract

Chitin, abundant in nature, is a renewable resource with many possible applications in bioengineering. Biosensors, capable of label-free and in-line evaluation, play an important role in the investigation of chitin synthesis, degradation and interaction with other materials. This work presents a comparative study of the usefulness of a chitin surface preparation, either on gold (Au) or on polystyrene (PS). In both cases the most common method to dissolve chitin was used, followed by a simple spin-coating procedure. Multi-parametric surface plasmon resonance (MP-SPR),

modeling of the optical properties of the chitin layers, scanning electron microscopy, and contact angle goniometry were used to confirm: the thickness of the layers in air and buffer, the refractive indices of the chitin layers in air and buffer, the hydrophobicity, the binding properties of the chitin binding domain (CBD) of *Bacillus circulans*, and the split-intein capture process. Binding of the CBD differed between chitin on Au versus chitin on PS in terms of binding strength and binding specificity due to a less homogenous structured chitin-surface on Au in comparison to chitin on PS, despite a similar thickness of both chitin layers in air and after running buffer over the surfaces. The use of the simple method to reproduce chitin films on a thin polystyrene layer to study chitin as a biosensor and for chitin binding studies was obvious from the SPR studies and the binding studies of CBD as moiety of chitinases or as protein fusion partner. In conclusion, stable chitin layers for SPR studies can be made from chitin in a solution of dimethylacetamide (DMA) and lithium chloride (LiCl) followed by spin-coating if the gold surface is protected with PS.

## Introduction

Chitin, along with its derivatives, is an increasingly popular biomaterial due to several useful properties, including biodegradability, low immunogenicity, non-toxicity, and biocompatibility [1-3]. Chitin is the main constituent of the exoskeletons of Arthropods, and is also found in fungal cell walls [3], cocoons of moths [4], diatoms, coralline algae, Molluscae, Protists, Polychaetes, within fish, [5] and marine and freshwater sponges [6, 7], and it is the second most abundant biopolymer after cellulose [3]. Chitin easily be processed in to a number of derivatives, *e.g*. chitosan; these have shown promising applications in a broad range of areas, including food science, medicine, agriculture [8], and the biomedical field [9].

Chitin is an insoluble linear polymer of aminoglucopyrans with extended linear chains of ß-1,4-linked N-acetylglucosamine residues (figure 1), and three polymorphs of this polysaccharide are known [10, 11]. It exists in three structural forms: α-, ß- and γ-chitin that have different mechanical properties depending on the arrangement of the polymer chains. The α-form represents an alternating antiparallel arrangement of polysaccharide chains (e.g. crustaceans [12]), the ß-form is a parallel chain arrangement (found e.g. in squid), and in the γ-form two parallel chains statistically alternate with an antiparallel chain (found e.g. in fungi) [4, 13]. The α-chitin isomorph is most abundant and formed by: enzymatic polymerization [14], *in*-vitro biosynthesis [15, 16], and recrystallization from solution [17]. Chitin is more than 50% acetylated, while chitosan is primarily deacetylated [11]. Shrimp chitin has been reported to be > 95% acetylated [18].

The use of chitin, and to a greater extent, chitosan films as constituents of biosensors have gained interest as the direct study of chitin is important in gaining insight into enzyme degradation pathways, interactions with natural composite materials (e.g., proteins and polysaccharides), and mechanisms behind biocompatibility and biofunctionality [19, 20]. Chitin and chitosan are useful transducer surface modifiers and found many applications as a electrochemical (bio-)senor component, for example in Pt disk electrodes for choline-sensing, supercapacitors [21] for nucleic acid analysis (e.g. DNA microarrays), immunosensors (e.g. biomarker analysis), enzyme activity, and detection of trace elements (for comprehensive reviews please read Suginta et al. *2013* [11] and Kim et al. *2015* [22]). In addition, chitin can be easily modified via its hydroxyl and acetylamido groups for future biosensor advancements. Chitin has advantageous mechanical properties, such as a high mechanical stability (tensile strengths between 38 – 146 MPa have been reported) and a high thermal stability (e.g. shrimp shell chitin's thermal degradation is between 290 – 440 °C), though these properties are underused in industry [5].

In order to create chitin surfaces with representative properties similar to its natural structure, chitin needs to be dissolved first, and then deposited onto the sensor surface. One approach is the use of biomimetic methods, for example to use naturally occurring biocomposites. For instance, instead of spin-coating chitin on a silicon surface [23], silica-chitin based biocomposites, or other biocomposites, could be used and it is available from various sources and can even be obtained in-vitro [24-28]. A newly emerging area is the use of natural sources from environments where life is found under extreme heat or pressure, also referred to as extreme biometrics [5]. The solubility of chitin depends on the pH and ionic strength of the solvent used and is influenced by the percentage and distribution of acetylated (and deacetylated) moieties along the backbone of the polysaccharide [11]. It is high in crystallinity and does not dissolved in hot water [27]. The most common method to solubilize chitin is the use of dimethylacetamide (DMA) and lithium chloride (LiCl), already demonstrated at the beginning of the last century [29, 30]. Recrystallizing chitin from a 5% LiCl in DMA solution by precipitation had an essentially crystalline form as the chitin prior to solution (be it the α- or the ß-form), though the α-form can be slightly disordered [23]. Alternative methods for the solubilization of chitin have been reported, such as using other polar solvents: LiCl/*N*-methyl-2-pyrolidone, chloride dihydrate/methanol [31], and hexofluoroisopropanol (HFIP) [32], or ionic liquids, such as 1-allyl-3-methylimidazolium bromide ([Amim]Br), [$C_2$mim][OAc], and 1-butyl-3-methylimidazolium acetate [31]. Thin chitin films are interesting for studies of chitinases which can convert chitin into cheap products such as N-acetylglucosamine for biomedical use [2]. Chitin films on silica surfaces by means of spin-coating were 50 nm thin, but rough [33]. Furthermore, a smooth, thin layer of amorphous chitin was obtained after the spin coating of trimethylsilyl chitin onto a silica or gold surface after which the films were regenerated to amorphous chitin [2].

One analytical method, which is highly compatible with thin layers is surface plasmon resonance (SPR). It is a highly sensitive, non-invasive, and label-free technique that is used extensively for

surface interaction studies between polymers and proteins [34]. In addition, it has been used to evaluate a chitin-coated surface in the past using ionic liquids as a solvent [2]. However, no simple protocol for the preparation of thin chitin layers using DMA/LiCl as solvent on SPR gold sensors has been established yet.

In this contribution, we demonstrate that the precipitation of chitin, derived from shrimp shell, using the common DMA/LiCl solvation method onto a gold surface for subsequent SPR analysis poses a challenge due to the surface properties of gold, but can be protected by an additional coating of polystyrene prior to chitin coating. The composition, thickness, available binding surface, surface hydrophobicity, and ability to interact with a CBD of chitin were characterized with multi-parametric surface plasmon resonance (MP-SPR), scanning electron microscopy (SEM), and contact angle goniometer with two different SPR sensors: bare gold and a polystyrene coated gold. The binding constants of a chitin binding domain fused to a split intein and its split intein counterpart were determined for both systems, as well as the differences in behavior of chitin on gold versus polystyrene after spin coating.

## Methodology

### *Materials*

Unless specifically mentioned all commercial chemicals (dimethylacetamide (DMA), LiCl, hexofluoroisopropanol (HFIP), EDTA, DTT, $NaN_3$, triethanolamine hydrochloride (TEA), Tris, sodium chloride, ampicillin, Isopropyl β-D-1-thiogalactopyranoside (IPTG), magnesium chloride, and chitin polymers derived from shrimp shell (C7170, lot: 051M7013V) were obtained from Sigma-Aldrich (USA) with a reported acetylation degree of 98 ± 12 % [18]. Reaction buffers and media used were composed as follows: Buffer A: 100 mM TEA, 1 mM EDTA, 1mM DTT, 1mM $NaN_3$, pH 7.6 (at 25° C). Buffer B: 20 mM TEA, 1 mM EDTA, 1mM DTT, 1mM $NaN_3$, pH 8 (at

125 25° C). Buffer C: 20 mM Tris/HCl, 100 mM sodium choride, pH 7.0 (at 25° C). Buffer D: 50 mM
126 Tris/HCl, 50 mM NaCl, pH 8.0 (at 25°C). DNAse and RNAse were obtained from Epicentre
127 (Madison, WI, USA). Phenylmethylsulfonyl fluoride (PMSF) was obtained from ThermoFisher
128 Scientific, USA. EnPressoB medium was obtained from BioSilta Ltd. (U.K); currently available via
129 EnPresso GmbL (Berlin, DE).
130
131 *DNA methods*
132 The eGFP gene from the pEGFP-C1 plasmid (Clontech, USA) was cloned into the pTYB21
133 plasmid, containing the *Sce*VMA1 gene (NEB, USA) to yield the eGFP-*Sce*VMA1 Intein-CBD
134 construct with use of Gibson Assembly® (NEB, USA) according to manufacturer's instructions.
135 The eGFP gene was also cloned into a pMMRSF17 plasmid that contained the NpuDnaE Intein
136 gene in the same way (the full construct was a gift from Hideo Iwai based on Addgene plasmid #
137 20178). In order to generate the CBD-NpuDnaE$_{N\Delta16}$ gene, the CBD of the chitinase A1 (CBD$_{ChiA1}$)
138 enzyme of *Bacillus circulans* WL-12 was isolated from the pTYB21 plasmid (NEB, USA) using the
139 following primers in a gradient-PCR reaction using Dynazyme II polymerase (ThermoFisher
140 Scientific, USA):
141 '5-GGAATTCCATATGACAAATCCTGGTGTATC-3' and
142 5'-GGATCCGAATTCTTGAAGCTGCCACAA-3' (fragment A) and the NpuDnaE$_{N\Delta16}$ gene
143 isolated from the pMMRSF17-NpuDnaE with primers
144 5'-GAATTCGGATCCGCCTTAAGCTATGAAACGAA-3' and
145 5'-CGTTAAGCTTATTGAAGCTGCCACAAGG-3' (fragment B). The last primer introduced a
146 mutation (Cys → Ala) at position one of the NpuDnaE$_{N\Delta16}$ gene and a linker sequence (EFGS)
147 between the CBD and NpuDnaE$_{N\Delta16}$ in the final construct in pET21a (see below). In order to
148 generate the NpuDnaE$_{C16}$_ eGFP gene, the NpuDnaE$_{C16}$ was isolated from the pMMRSF17-
149 NpuDnaE plasmid using primers 5'-GGAATTCCATATGGGTCATAATTTTGCACTC-3' and

150 5'-CCCTTGCTCCCATATTAGAAGCTATGAAG-3' (fragment C) and the eGFP gene was
151 isolated from pTYB21-eGFP-Intein-CBD plasmid described above with primers
152 5'-TCATAGCTTCTAATATGGTGAGCAAGGGCGA-3' and
153 5'-TTTCAAGCTTTTACTTCTACAGCTCGTCCATGC-3' (fragment D). In an overlap extension
154 gradient-PCR (42° C – 60° C; 15 cycles) fragments A and B were combined with use of Dynazyme
155 II polymerase (ThermoFisher Scientific, USA). Fragments C and D were combined in similar way
156 (38° C - 45° C; 15 cycles). Faint bands in the latter were amplified with PCR and all reactions were
157 cleaned up with NucleoSpin® Gel and PCR Clean-up columns (Macherey-Nagel, DE). The CBD-
158 NpuDnaE$_{N\Delta16}$ gene and the NpuDnaE$_{C16}$– eGFP gene were then separately cloned into pET21a
159 expression vectors (Novagen, Merck KGaA, USA) after digestion with NdeI and HindIII
160 (ThermoFisher Scientific, USA) and ligation with T4 ligase (ThermoFisher Scientific, USA). The
161 complete DNA sequences of all genes were verified by gene sequencing (GATC, DE). *Escherichia*
162 *coli* NEB5-alpha competent cells (New England Biolabs, USA) were transformed and used for
163 plasmid propagation [35]. Plasmids were then transformed separately to *E. coli* strain BL21(DE3)
164 (Invitrogen, USA) for protein production.
165
166 *Protein expression and purification*
167 Expression of eGFP-*Sce*VMA1 Intein-CBD, CBD-NpuDnaE$_{N\Delta16}$ and NpuDnaE$_{C16}$-eGFP was
168 carried out in BL21(DE3) *E. coli* cells. First the transformants were grown o/n in LB Medium with
169 100 µg/ml ampicillin and 1% (w/v) glucose at 30°C from glycerol stocks; 2 ml o/n culture was used
170 to inoculate 50 ml of EnPressoB medium [36] with 100 $\mu$g/ml ampicillin at 30° C; 225 rpm (1"
171 amplitude shaker) according to manufacturer's instructions in high yield flasks [37]. Cells were
172 induced with 0.4 mM IPTG after 24 h and grown for another 24 h under the same conditions. Cells
173 were separated from the media via centrifugation (16 000 * g for 15 min) and then lysed by freezing
174 o/n at -20° C in the presence of DNAse (2.5 U/ml), RNAse (2.5 U/ml), Lysozyme (15 µg/ml), 0.1

175 mM PMSF (ThermoFisher Scientific, USA), and $MgCl_2$ in buffer D. The insoluble fraction was
176 removed by centrifugation (15 min at 9000 * g). The soluble protein fraction of CBD-NpuDnaE$_{N\Delta16}$
177 was loaded onto a 1 ml HiTrap DEAE FF column (GE healthcare USA) and eluted with buffer D at
178 incremental sodium chloride concentrations (100 mM, 150 mM, 200 mM, 250 mM, 500 mM). The
179 soluble pooled and concentrated protein fractions of NpuDnaE$_{C16}$-eGFP were heated at 70° C for 20
180 min, insoluble proteins removed by centrifugation (15 min; 16 000 *g), and the supernatant loaded
181 onto a size exclusion chromatography (SEC) HiLoad Superdex 200 prep grade filtration column
182 (GE healthcare, USA) using buffer A at 0.5 ml/min and protein fractions collected. The purity of all
183 fractions was evaluated by SDS-PAGE analysis (AnyKd gels, BioRad, USA) and fractions of the
184 target protein size were pooled. Eluate buffer A was replaced by buffer C using a 5kD NMWL
185 membrane at 2800 rpm (Merck-Millipore, USA). Protein concentrations were determined by $OD_{280}$;
186 Molecular weight and the ε was calculated with the ProtParam tool [38]. Hereafter we will
187 abbreviate CBD-NpuDnaE$_{N\Delta16}$ as CBD-IN$_N$ and NpuDnaE$_{C16}$-eGFP as IN$_C$-eGFP.
188
189 *Chitin coating*
190 Chitin was dissolved in DMA and 5% LiCl according to Austin P.R. (1984) [39] at a final
191 concentration of 0.1% (w/v). Bare gold sensors were spin-coated with 100 µl for 60 sec. at 3600
192 rpm; polystyrene coated senors (BioNavis Ltd., Ylöjärvi, Finland) were spin-coated by adding 100
193 µl to the sensor and then after 60 sec. the sensor was spin-coated at 60 sec. at 3600 rpm. The
194 sensors for SPR were used only once and spin-coated immediately before use, since LiCl leached
195 the gold off of the bare sensors after drying for longer periods at 60° C, and subsequent rehydrating
196 (fig. 1).
197 For scanning electron microscopy imaging the sensor was spin-coated prior to placement in
198 the vacuum chamber of the SEM microscope (application chamber) to determine the structure
199 before applying buffer. Sensors were then placed within 10 minutes in a SPR Navi™ 200

200 (BioNavis Ltd., Ylöjärvi, Finland) instrument and buffer was applied to the flow cell area at 20 °C,
201 with a flow rate of 20 µL/min. Samples were allowed to air-dry for at least 15 minutes before SEM
202 imaging of the flow cell area and the areas outside the flow cell under the same conditions.
203
204 *MP-SPR measurements*
205 Measurements were performed with a multi-parameter SPR Navi™ 200 (BioNavis Ltd., Ylöjärvi,
206 Finland) instrument. The setup was equipped with two incident laser wavelengths, 670 nm and
207 785 nm, two independent flow channels, inlet tubing and outlet (waste) tubing. Both of the flow
208 channels were measured in parallel with 670 nm and 785 nm incident light. The measurement
209 temperature was kept constant at 20 °C. The chitin coated SPR sensors were placed in the flow-cell
210 and SPR spectra were recorded in air after which buffer B was introduced into the flow-cell; the
211 flow rates used for the CBD-$IN_N$ interaction with chitin and for $IN_C$-eGFP interaction with CBD-
212 $IN_N$ were 20 µL/min. Chitin layer data in air was fitted in LayerSolver 1.2.1 (BioNavis, FIN) with
213 default parameters and simulation mode 0 for the Au layer, and mode 2 for all other layers. The
214 buffer (due to the presence of EDTA) prevented damage to the bare-gold sensors during the SPR
215 measurements due to removal of LiCl. The chitin coated gold and polystyrene sensor slides were
216 first subjected to buffer B for 10 – 30 min until a stable baseline was achieved. In the second phase,
217 CBD-$IN_N$ was injected into both flow channels for 8 minutes at increasing concentrations (490, 981,
218 1961, 3922, 7854 nM, equivalent to 10, 20, 40, 80, 160 ug/ml) to determine the binding constants
219 for both systems. Based on these results, CBD-$IN_N$ was bound to the new chitin coated sensors at
220 0.5 and 5 $\mu$g/ml of protein during a 5-minute injection. $IN_C$-eGFP protein was then injected in both
221 channels for 5 minutes at increasing concentrations (17.5, 175, 350, 701, 1401, 2803 nM, equivalent
222 to 0.5, 5.0, 10.0, 20.0, 40.0, and 80.0 $\mu$g/ml) to determine the binding constant of the split-intein
223 pair for both SPR sensors. The data was fitted in TraceDrawer software v1.6 (BioNavis, FIN &

224 Ridgeview Instruments, SWE) according to the OneToTwo model to obtain the association rates,
225 dissociation rates, and the binding constants after evaluations of other relevant models.
226
227 *Scanning Electron Microscopy*
228 SEM images were recorded using an FEI Quanta 250 Field Emission Gun Scanning Electron
229 Microscope under high vacuum ($< 6 \times 10^{-4}$ Pa) to prevent deterioration of the chitin layer due to
230 moisture in the air.
231
232 *Contact angle measurements*
233 Au, PS, Au-chitin, and Au-PS-chitin surfaces were prepared as described above. The Au sensor
234 surface was cleaned in two ways: (1) plasma treated as above and (2) boiled for 15 min in and $NH_3$
235 (30%)/$H_2O_2$ (30%)/$H_2O$ (1:1:5, v/v) oxidizing solution. A syringe and needle were washed with
236 70% ethanol and rinsed with fully deionized water (Milli-Q water) and the camera was adjusted
237 before each measurement. The shape of the water droplet on the surface was recorded with a CAM
238 200 optical contact angle meter (KSV instrument LTD) equipped with CCD video camera module
239 and the drop volume was constant during the whole measurement (static mode). The drop height
240 prior to the measurement was 200 pixels (approx. 8 $\mu$l of Milli-Q water), and recording started
241 automatically upon detection of the drop on the surface with a frame interval of 1 second for 60
242 frames. Contact angels were calculated according to the Young-Laplace fitting model using the
243 Attension theta 4.1.0 software (KSV instruments LTD). After the contact angle was stable (i.e. in
244 the case of Au and PS) with out chitin) the mean of frames from 45 second to 60 second was
245 calculated. For the contact angle of water on the chitin surfaces (dry or wet) the rate of the contact
246 angle change was different, but lower than 1° at the end of each measurement.
247
248 **Result and Discussion**

249

250 **Surface properties of the spin coated sensors**

251 We observed in PS 96-well plates (Corning, USA) with (a) 0.1% chitin solution in DMA/5% LiCl
252 and (b) 0.1% chitin solution in HFIP [32], and subsequently dried overnight in an oven with a fan at
253 60° C, that (i) chitin precipitated out of DMA/5% LiCl formed large crystal structures and that non-
254 reproducible amounts remaining in the wells after washing with vigorously with water, (ii) chitin
255 precipitated out of HFIP formed a layered gel, which after upon adding water detached from the PS
256 surface, (iii) eGFP-intein-CBD (IMPACT$^{TM}$ kit [40], New England Biolabs, USA) was able to bind
257 and release eGFP according to the kit instructions from crude cell lysates (data not shown). We also
258 used the eGFP-intein-CBD crude lysate to determine that the CBD does not bind to Au (data not
259 shown). Therefore, in order to study chitin binding and the binding/release of split-inteins, SPR Au
260 sensors coated with chitin were initially dried overnight at 60° C. However, the gold was leached
261 from the retrieved SPR sensors after the experiment (i.e. the gold and chitin layer detached from the
262 glass surface; figure 2). For this reason, all binding experiments here reported were performed with
263 buffer B in order to scavenge the LiCl from the surface. In addition, PS coated Au SPR sensors
264 were utilized as well and directly compared. An alternative method, as presented by Kittle et al.
265 *2012* [2] for preparing chitin-SPR sensors produces excellent uniform chitin layer, however the
266 methods we propose requires less experimental steps, and therefore simplifies the use of chitin as a
267 substrate for SPR sensors.

268

269 The cleaning protocol of gold has an effect on the hydrophobicity of the surface (table 1). Au
270 surfaces boiled for 15 min in a $NH_3$ (30%)/$H_2O_2$ (30%)/$H_2O$ (1:1:5, v/v) oxidizing solution were
271 more hydrophobic than plasma cleaned surfaces. Since it had been shown that: (i) more oxidized
272 gold surfaces are more hydrophilic [41], and (ii) the intention of spin-coated chitin is to interact
273 with its surface more effectively by sampling more hydrogen bonds outside its internal structure

[42, 43] all surfaces were plasma treated prior to spin coating. The polystyrene surface can be easily oxidized through plasma treatment [44].

The hydrophobicity of the surfaces was evaluated with a goniometer to determine the contact angle of a water droplet during the first 60 seconds of contact. The chitin surfaces were either spin-coated and then dried under a nitrogen flow or spin-coated, wetted with a few drops of buffer B and then dried under a nitrogen flow (Chitin in air or Chitin in buffer in table 1 respectively). On the Au and PS surfaces the water droplet formed was stable throughout the measurement (figure 3), while the water droplet on pre-wetted chitin surfaces immediately spread over the surface. On dried chitin surfaces the water droplet behaved differently than on the Au-chitin surface or the PS-chitin surface. In Au-chitin the contact angle decreased under 10° after 2 seconds and reached a value below 1° within 30 seconds, while the contact angle of a water droplet on PS-chitin was initially higher, the droplet spread slower, and a thicker water layer remained (figure 3).

The thickness of the chitin layers directly after spin-coating was determined with SPR in air (table 1 & figure 4) by using the Layersolver software based on Granqvist *et al*. [45]. First the Au layer was measured and modelled (figure 4A) after which chitin was spin-coated on the surface and the thickness determined. Due to the high thickness waveguide-fitting for one wavelength would suffice, but the measured SPR spectra at both wavelengths fit the models well. Therefore, we always fitted both wavelengths in one model to enhance accuracy. The PS coated Au sensor was determined in similar fashion: first the thickness of PS was determined, after which similar model parameters of the chitin on Au-model were applied to obtain the Au-PS models in air. From the models it is clear that the layer's refractive indices ($n$) in air are much lower than reported for shrimp chitin, which is reported at $n = 1.61$ [46]. This behaviour has previously been observed for spin-coated chitin for which the refractive index can vary greatly between $n = 1.30$ - 1.47 depending

299 on the solvent used [47]. In our case, buffer B at pH 8.0, needed for the protein stability to study
300 their interactions with chitin, may have had an influence on the refractive index of spin-coated
301 chitin.
302
303 In order to determine the refractive index of chitin after the introduction of buffer, the total internal
304 reflection (TIR) angle was manually fitted in the Layersolver software for the Au-chitin layer.
305 Based on the principle that the bulk effect in the SPR curves is constant, while we assume the Au
306 layer to be constant, the changes in the TIR angle-shape during the stabilization of the TIR angles
307 and overall SPR signal are indicative to the changes in thickness. In addition, it is known that
308 hydrogels, such as polyacrylamide gels have a lower refractive index than the starting material [48].
309 We observed a hydrated state after washing the spin-coated chitin surface with buffer B prior to the
310 contact angle measurements (fig. 3). Overall, the refractive index of chitin can differ greatly
311 depending on how the polymers are precipitated [47]. We disagree with the assumption of Kittle *et*
312 *al*. [2] that the refractive index of spin-coated chitin is 1.51 and thus we used the change of the
313 shape of the TIR angle to fit the theoretical maximum thickness (fig. 5) and a resulting *n*-value for
314 both wavelengths for the Au-chitin layer. Thereafter, we fitted the minimal thickness and refractive
315 index for the experimentally SPR curves manually with the Layersolver software. The results are a
316 realistic range of the thickness and refractive indices for both wavelengths. Since we did not
317 observe the phenomena of the TIR angle-shape changing after the introduction of buffer B over
318 time regarding the Au-PS-chitin surface, we took the minimum and maximum refractive indices
319 determined with the Au-chitin models in buffer, and used them as initial values to manually fit the
320 experimental data as above to find a realistic range of the thickness and *n*-values for the Au-PS-
321 chitin layer in buffer. All four resulting models fit the experimental data the best (fig. 4C and 4F).
322 In addition, an apparent change in the thickness of the PS layer had to be corrected for in the
323 models. Therefore we fitted the sensor parameters simultaneously with the layer (table 1). It is

known that DMA damages PS [49], however as we observed in Scanning Electron Microscopy (SEM) imaging (fig. 8C and 8D), enough PS remained during the short period of interaction with DMA in the spin-coating process. Since DMA is removed during spin-drying [50] and the PS is not severely damaged during the spin-coating process, the deposited LiCl on the surface is not interacting with Au as observed in figure 8C.

Upon further visual inspection with SEM of the spin coated chitin layers, at first glance chitin on gold or chitin on PS before SPR measurements appear to have similar structures, though appear to be cruder on the Au-PS layer (fig. 8A and 8B). However, after one hour under normal atmospheric conditions at room temperature, chitin on gold presented large build-up structures not observed in the Au-PS layer. As seen in figure 2, this is most likely the result of the electrochemical reaction between Au and Li [51]. In order to remove the LiCl from the dried chitin layer, EDTA was added to a buffer (Buffer B). The response in the SPR sensorgram upon introduction of the liquid phase in either buffer D (without EDTA) or Buffer B (including EDTA) differed. Upon contact with buffer D, the base line in the SPR sensorgram sloped slowly down and stabilized after 15-20 minutes. In the case of the EDTA containing buffer the baseline dropped immediately and then stabilized within 20 minutes on the Au surface due to changes in the thickness (fig. 5), while the baseline is stable within seconds on the Au-PS surface. The SPR sensors with a stable baseline in buffer B were then transferred, while air-drying, within 15 minutes to the vacuum chamber of the SEM equipment (fig. 8E and 8F). The cubical structures on the Au-PS surface are clearly sodium chloride crystals [52], while it is unclear what the large macrostructures are on the Au surface at this magnification. In-between the macrostructures chitin can be seen at higher magnification (fig. 8G and 8I). On Au, chitin appears to be connected at the edge of the macrostructures (fig. 8G arrow), while chitin on the Au-PS surface appears to be more uniform.

349 Chitin responded to the atmospheric conditions rather rapidly, most likely due to moisture in the air,
350 since when the Au-PS surface was directly placed in vacuum (< 30 seconds; fig. 9A and 9C) or
351 after 5 minutes (fig. 9B and 9D), the spin-coated surfaces looked very different. At lower
352 magnification we observed geometric patterns appear after a few minutes (fig. 9B), which were
353 stable on the Au-PS surfaces for at least an hour (fig. 8B). At higher magnification we observed a
354 flakey structure (fig. 9C) at first and a more uniform geometrical surface of the spin-coated surface
355 after 5 minutes (fig. 9D).
356
357 The chitin layers on Au or Au-PS in air were similar when observed with SEM and their layer
358 thickness was nearly the same. The differences after exposure of buffer B, at a flow of 20 μL/min in
359 the SPR flow-cell, were evident; while the surface of Au looks damaged and not uniform, chitin on
360 Au-PS appears smoother. The range of the chitin layer's thickness on Au-PS was slightly lower that
361 chitin on Au. Our layers were in the same range as earlier reported thicknesses [2].
362
363 **Differences in binding properties**
364 The surfaces (Au spin-coated with chitin and Au coated with PS and spin-coated with chitin) did
365 not only differ in surface properties, the chitin binding domain of *Bacillus circulans* ($CDB_{ChiA1}$)
366 showed different binding characteristics to chitin as well (table 2 & figure 6). $CDB_{ChiA1}$ fused to the
367 split-intein $NpuDnaE_{N\Delta 16}$ ($CBD\text{-}IN_N$) was titrated to both surfaces at increasing concentrations
368 (figure 6). The resulting sensorgrams were then fitted to different models using the TraceDrawer
369 software until the best fit with the lowest variation (Chi-Square) was calculated. For both
370 experiments the best fitting model was a OneToTwo model [53]. This model indicates that the
371 $CBD\text{-}IN_N$ protein binds specifically and nonspecifically to the chitin surface.
372

373 The chitin-binding domain bound very tightly to both chitin layers and we did not observe a
374 dissociation phase, however there was a clear difference in binding to spin-coated chitin on gold
375 versus spin-coated chitin on a thin PS layer. Not only was the binding of the CBD to chitin on PS
376 must stronger, the binding rates were higher, and binding was more specific (table 2 and figure 6).
377
378 The binding constants for various CBDs have been mainly determined by means of solution
379 depletion studies and ICT (table 3). Though the theoretical differences between the solution
380 depletion method and SPR had been thoroughly described [54, 55], to the best of our knowledge we
381 could find only one direct comparison of both methods of a protein interaction with a
382 polysaccharide: the study of BSA binding to cellulose. When the binding constant of BSA to
383 cellulose was determined by isothermal titration calorimetry (ITC) and the solution depletion
384 method at pH 7-7.5, the authors [56] found a $K_d$ of 10 μM or 0.66 mg/ml by ICT and 38 μM or 2.53
385 mg/ml by solution depletion followed by UV spectroscopy, with a $B_{max}$ of 0 (ICT) or 36.3 mg
386 (solution depletion & UV) BSA/gram cellulose extrapolated from their graphs for 0% pyridinium-
387 grafted chitin nanocrystals, while in an earlier SPR study [57], at pH 7-7.5, about 0.5 mg/cm$^2$ was
388 bound to the sensor surface. This was an equivalent to a $B_{max}$ of about 0.018 mg BSA/gram of
389 cellulose. The binding kinetics were not determined. The $B_{max}$ determined with ICT of zero is close
390 to the value determined with SPR and the difference may in the margin of error. The $B_{max}$
391 determined with the solution depletion method was over 2000-fold higher than with SPR. Though
392 the ease of the solution depletion method cannot be denied, SPR offers a more detailed analysis of
393 the surface properties and is more sensitive. On the other hand, as pointed out by Lombardo *et al.*
394 [56], during SPR measurements, a constant flow of BSA is supplied over immobilized cellulose,
395 forcing the protein to adsorb to a higher extent. ITC seems to be closer in correlation with SPR than
396 the depletion method. Therefore, when comparing the values in table 3 derived from the solution
397 depletion method with SPR, we can expect lower $K_d$ values with at least one order of magnitude. In

398 addition, as determined by Hashimoto *et al*. [62], $CBD_{CHA1}$ binds only to insoluble chitin, such as
399 shrimp chitin powder. This may explain the even higher affinity (i.e. smaller $K_d$) in the case of
400 chitin spin-coated on the polystyrene surface, since the chitin layer formed a stable, uniform layer
401 immediately upon the introduction of buffer B. Based on these observations, and an earlier one
402 [23], we assume that the chitin structures mimic shrimp shell well enough for the study of chitin
403 and its interaction with biomolecules, such as chitinases.
404
405 The chitin structure had an effect on its interaction with CBD-$IN_N$ and $IN_C$-eGFP. Though in both
406 the Au-chitin and the Au-PS-chitin surface the CBD-$IN_N$ and $IN_C$-eGFP interaction followed a
407 capture and collapse mechanism the kinetic data fitting of our SPR experiments (Fig. 7) confirmed
408 by the observation of the single binding phase observed with stopped-flow fluorescence [58]. The
409 calculated binding constants were higher for the Au-chitin surface, but with a higher specific
410 binding. On the other hand, on the Au-PS-chitin surface, the intein pair bound more tightly, but
411 showed some non-specific binding as well. The binding constant of the split intein pair was in
412 general higher than observed previously, except for Au-PS with a 0.25 nM CBD-$IN_N$ solution
413 titrated to the surface, before introduction of the split intein pair: 1.2 nM [58] and 1.6 nM (this
414 study; table 2).
415
416 **Conclusions**
417 In summary, this work highlights the differences between two different sensor chips and their
418 implication for the study of chitin binding proteins and chitin binding domain as an immobilizing
419 agent for the study of split-inteins. The spin-coated films of chitin used with DMA/LiCl as a solvent
420 is damaging for the gold layer, despite the use of EDTA in the SPR running buffer. Polystyrene on
421 a gold sensor protects the gold layer from the solvent well enough for a homogeneous chitin layer to
422 form during the spin-coating process. SPR is a suitable tool to determine the thickness of the spin-

423 coated layers before applying buffer, during the introduction of buffer to the system, and to
424 investigate the binding behavior of protein binding to the sensors. The utility of
425 chitin films as biosensors is evident from the chitin binding domain binding studies. SPR is highly
426 sensitive and new surface plasmon resonance surfaces based on copper [65] or zinc oxide [66] are
427 an interesting avenue for future applications when combined with biomimetic approaches based on
428 chitin metal composites of the same metals (e.g. copper [7] or zinc oxide [67]). The results we
429 presented here are expected to enable studies of chitin layer properties and interactions with
430 biomolecules without the use of labels in real-time with high sensitivity.
431

432 **Acknowledgments**

433 This work was funded and supported by the Academy of Finland projects 272597, 303884, and
434 137053. We thank Dr. Hideo Iwai for providing us with the plasmid containing the NpuDnaE gene.
435 We thank Dr. Ilya Belevich from the Electron Microscopy Unit, Institute of Biotechnology, of the
436 University of Helsinki, Finland for his technical guidance with scanning electron microscopy and
437 image analysis. We also would like to thank Erja-Liisa Piitulainen and Leena Pietilä for their kind
438 laboratory assistance, and Regina Casteleijn-Osorno of AaltoEE and Dr. Alex Bunker of the Drug
439 Research Program at the University of Helsinki for comments that greatly improved the manuscript.
440

441 **References**

442 1. C.K.S. Pillai, W. Paul, C.P. Sharma, Chitin and chitosan polymers: Chemistry, solubility and
443 fiber formation, Prog. Polym. Sci. 34 (2009) 641–678.
444 2. J.D. Kittle, C. Wang, C. Qian, Y. Zhang, M. Zhang, M. Roman, J.R. Morris, R.B. Moore, A.R.
445 Esker, Ultrathin Chitin Films for Nanocomposites and Biosensors, Biomacromolecules, 13
446 (2012) 714–718. DOI: 10.1021/bm201631r

3. M.N.V.R. Kumar, A review of chitin and chitosan applications, React. Funct. Polym. 46 (2000), 1 – 27.
4. M. Kaya, M. Mujtaba, H. Ehrlich, A.M. Salaberria, T. Baran, C.T. Amemiya, R. Galli, L. Akyuz, I. Sargin, J. Labidi, On chemistry of gamma-chitin, Carbohydr Polym, 176, (2017), 177-186.
5. M. Wysokowski, I. Petrenko, A.L. Stelling, D. Stawski, T. Jesionowski, H. Ehrlich H, Poriferan Chitin as a Versatile Template for Extreme Biomimetics. Polymers, 7 (2015) 235-265.
6. M. Wysokowski, V.V. Bazhenov, M.V. Tsurkan, R. Galli, A.L. Stelling, H. Stocker, S. Kaiser, E. Niederschlag, G. Gartner, T. Behm, M. Ilan, A.Y. Petrenko, T. Jesionowski, H. Ehrlich, Isolation and identification of chitin in three-dimensional skeleton of Aplysina fistularis marine sponge, Int J Biol Macromol, 62 (2013), 94-100.
7. I. Petrenko, V.V. Bazhenov, R. Galli, M. Wysokowski, J. Fromont, P.J. Schupp, A.L. Stelling E. Niederschlag, H. Stoker, V.Z. Kutsova, T. Jesionowski, H. Ehrlich , Chitin of poriferan origin and the bioelectrometallurgy of copper/copper oxide. Int J Biol Macromol, 104 (2017) 1626-1632.
8. B.K. Park, M.M. Kim, Applications of Chitin and Its Derivatives in Biological Medicine. Int. J. Mol. Sci., 11(12) (2010) 5152–5164 http://doi.org/10.3390/ijms11125152
9. P. Jolles, R.A.A. Muzzarelli, Chitin and Chitinases. Jollès P, Muzzarelli RAA, editors. Birkhauser Verlag; Basel, Switzerland, 1999.
10. A. Anitha A, S. Sowmya, P.T.S. Kumar, S. Deepthi, K.P. Chennazhi, H. Ehrlich, M. Tsurkan, R. Jayakumar, Chitin and chitosan in selected biomedical applications. Progress in Polymer Science, 39 (2014), 1644-1667.
11. W. Suginta, P. Khunkaewla, A. Schulte, Electrochemical biosensor applications of polysaccharides chitin and chitosan. Chem Rev, 113 (2013) 5458-5479.

12. I. Younes, M. Rinaudo, Chitin and chitosan preparation from marine sources. Structure, properties and applications. Mar Drugs, 13 (2015) 1133-1174.
13. K.M. Rudall, W. Kenchington, The Chitin System, Biological Reviews, 48 (1973), 597–633. doi:10.1111/j.1469-185X.1973.tb01570.x
14. J. Sakamoto, J. Sugiyama, S. Kimura, T. Imai, T. Itoh, T. Watanabe, S. Kobayashi, Artificial chitin spherulites composed of single crystalline ribbons of α-chitin via enzymatic polymerization. Macromolecules. 33 (2000) 4155–4160.
15. J. Ruiz-Herrera, V.O. Sing, W.J. van der Woude, S. Bartnicki-Garcia, Microfibril assembly by granules of chitin synthetase. Proc. Natl. Acad. Sci. USA, 72 (1975) 2706–2710.
16. S. Bartnicki-Garcia, J. Persson, H. Chanzy, An electron microscope and electron diffraction study of the effect of calcofluor and congo red on the biosynthesis of chitin *in vitro*. Arch. Biochem. Biophys. 310 (1994) 6–15.
17. W. Helbert, J. Sugiyama, High-resolution electron microscopy on cellulose II and α-chitin single crystals, Cellulose, 5 (1998) 113–122.
18. C.P. Moraru CP, V. Ostafe, Preliminary results on estimation of the degree of acetylation of chitosan by UV spectrophotometry, New Front Chem, 24 (2015), 125-133.
19. G. Vaaje-Kolstad, B. Westereng, S.J. Horn, Z. Liu, H. Zhai, M. Sørlie, V.G.H. Eijsink, Science, 330 (2010) 219–222.
20. S. Boddohi, M.J. Kipper, Engineering Nanoassemblies of Polysaccharides, Adv. Mater. 22 (2010) 2998–3016
21. I. Stepniak, M. Galinski, K. Nowacki, M. Wysokowski, P. Jakubowska, V.V. Bazheno, T. Leisegang, H. Ehrlich, T. Jesionowski, A novel chitosan/sponge chitin origin material as a membrane for supercapacitors - preparation and characterization. Rsc Advances, 6 (2016) 4007-4013.

22. E. Kim, Y. Xiong, Y. Cheng, H.C. Wu, Y. Liu, B.H. Morrow, H. Ben-Yoav, R. Ghodssi, G.W. Rubloff, J.N. Shen, W.E. Bentley, X. Shiet, G.F. Payne, Chitosan to Connect Biology to Electronics: Fabricating the Bio-Device Interface and Communicating Across This Interface. Polymers, 7 (2015) 1-46.
23. B. Focher, A. Naggi, G. Torri, A. Cosani, M. Terbojevich, Structural differences between chitin polymorphs and their precipitates from solutions—evidence from CP-MAS C-NMR, FT-IR and FT-Raman spectroscopy, Carbohydr Polym., 17 (1992) 97–102.
24. H. Ehrlich, S. Heinemann, C. Heinemann, P. Simon, V.V. Bazhenov, N.P Shapkin, R. Born, K.R. Tabachnick, T. Hanke, H. Worch, Nanostructural organization of naturally occurring composites - Part I: Silica-collagen-based biocomposites. Journal of Nanomaterials (2008) Article ID 623838, 8 pages, doi:10.1155/2008/623838.
25. H. Ehrlich H, Chitin and collagen as universal and alternative templates in biomineralization. International Geology Review, 52 (2010), 661-699.
26. E. Brunner E, P. Richthammer, H. Ehrlich, S. Paasch, P. Simon, S. Ueberlein, K.H. van Pee, Chitin-Based Organic Networks: An Integral Part of Cell Wall Biosilica in the Diatom Thalassiosira pseudonana. Angewandte Chemie-International Edition, 48 (2009), 9724-9727.
27. M. Wysokowski, K. Materna, J. Walter, I Petrenko, A.L. Stelling, V.V. Bazhenov, L. Klapiszewski, T. Szatkowski, O. Lewandowska, D. Stawski, S.L. Molodtsov, H. Maciejewski, H. Erhlich, T. Jesionowski, Solvothermal synthesis of hydrophobic chitin-polyhedral oligomeric silsesquioxane (POSS) nanocomposites. Int J Biol Macromol, 78 (2015) 224-229.
28. M. Wysokowski, T. Behm, R. Born, V.V. Bazhenov, H. Meissner, G. Richter, K. Szwarc-Rzepka, A. Makarova, D. Vyalikh, P. Schupp, T. Jesionowski, H. Erhlich. Preparation of chitin-silica composites by in vitro silicification of two-dimensional Ianthella basta demosponge chitinous scaffolds under modified Stober conditions. Mater Sci Eng C Mater Biol Appl, 33 (2013) 3935-3941.

29. v. P.P. Weimarn, Eine allgemein anwendbare Methode, Fibroin, Chitin, Kasein und ähnliche Substanzen nit Hilfe kozentrierter wässeriger Lösungen leicht löslicher und stark hydratisierter Salze in den plastischen Zustand und in den Zustand kolloider Lösung überzuführen. Kolloid-Zeitschrift, 40 (1926) 120-122.
30. v. P.P. Weimarn, Kolloide Auflösung hochmolekularer Verbindungen durch sehr leicht lösliche, stark hydratisierte Substanzen. Kolloid-Zeitschrift, 42 (1927) 134-140.
31. X. Shen, J. L. Shamshina, P. Berton, G. Gurauc and R. D. Rogers, Hydrogels based on cellulose and chitin: fabrication, properties, and applications, Green Chem., 18 (2016) 53-75.
32. C. Zhong, A. Cooper, A. Kapetanovic, Z. Fang, M. Zhang and M. Rolandi, A facile bottom-up route to self-assembled biogenic chitin nanofibers. Soft Matter, 6 (2010) 5298–5301.
33. Y. Kikkawa, H. Tokuhisa, H. Shingai, T. Hiraishi, H. Houjou, M. Kanesato, T. Imanaka, T. Tanaka, Interaction Force of Chitin-Binding Domains onto Chitin Surface, Biomacromolecules. 9 (2008) 2126– 2131.
34. R.B.M. Schasfoort, A.J. Tudos, Handbook of Surface Plasmon Resonance, The Royal Society of Chemistry, Cambridge, 2008.
35. J. Sambrook, D.W. Russell, Molecular cloning. A laboratory manual, 3rd edition, Cold spring harbor laboratory press, 2001.
36. J. Panula-Perälä, J. Šiurkus, A. Vasala, R. Wilmanowski, M.G. Casteleijn, P Neubauer, Enzyme controlled glucose auto-delivery for high cell density cultivations in microplates and shake flasks, Microbial Cell Factories, (2008) 7, 31. http://doi.org/10.1186/1475-2859-7-31
37. K. Ukkonen, A. Vasala, H. Ojamo, P. Neubauer, High-yield production of biologically active recombinant protein in shake flask culture by combination of enzyme-based glucose delivery and increased oxygen transfer. Microbial Cell Factories, (2011) 10, 107. http://doi.org/10.1186/1475-2859-10-107

38. E. Gasteiger, C. Hoogland, A. Gattiker, S. Duvaud S, M.R. Wilkins, R.D. Appel, A. Bairoch, Protein Identification and Analysis Tools on the ExPASy Server, (In) John M. Walker (ed): The Proteomics Protocols Handbook, Humana Press, 2005, pp. 571-607

39. P.R. Austin. Chitin solvents and solubility parameters. J.P. Zikakis (Ed.), Chitin and chitosan and related enzymes, Academic Press, Inc., Orlando, 1984, pp. 227-237

40. S. Chong, F.B. Mersha, D.G. Comb, M.E.Scott, D. Landry, L.M. Vence, F.B. Perler, J. Benner, R.B. Kucera, C.A. Hirvonen, J.J. Pelletier, H. Paulus, M.Q. Xu, Single-column purification of free recombinant proteins using a self-cleavable affinity tag derived from a protein splicing element, Gene, 192, (1997) 271-281. Doi: 10.1016/S0378-1119(97)00105-4.

41. K. W. Bewig, W. A. Zisman, The Wetting of Gold and Platinum by Water, J. Phys. Chem., 69 (1965) 4238-4242. DOI: 10.1021/j100782a029

42. V.L. Deringer, U. Englert, R. Dronskowski, Nature, Strength, and Cooperativity of the Hydrogen-Bonding Network in α-Chitin, Biomacromolecules, 17 (2016) 996-1003. DOI: 10.1021/acs.biomac.5b01653

43. T. Kameda, M. Miyazawa, H. Ono, M. Yoshida, Hydrogen Bonding Structure and Stability of $\alpha$-Chitin Studied by $^{13}$C Solid-State NMR. Macromol. Biosci., 5 (2005) 103–106. doi:10.1002/mabi.200400142

44. C. C. Dupont-Gillain, Y. Adriaensen, S. Derclaye, P. G. Rouxhet, Plasma-Oxidized Polystyrene: Wetting Properties and Surface Reconstruction. Langmuir, 16 (2000) 8194-8200. DOI: 10.1021/la000326l

45. N. Granqvist, H. Liang, T. Laurila, J. Sadowski, M. Yliperttula, T. Viitala, Characterizing Ultrathin and Thick Organic Layers by Surface Plasmon Resonance Three-Wavelength and Waveguide Mode Analysis. Langmuir, 29 (2013) 8561-8571. DOI: 10.1021/la401084w

46. D.E. Azofeifa, H.J. Arguedas, W.E. Vargas, Optical properties of chitin and chitosan biopolymers with application to structural color analysis, Optical Materials, 35 (2012) 175-183.

47. K. Manabe, C. Tanaka, Y. Moriyama, M. Tenjimbayashi, C. Nakamura, Y. Tokura, T. Matsubayashi, K.H. Kyung, S. Shiratori, Chitin Nanofibers Extracted from Crab Shells in Broadband Visible Antireflection Coatings with Controlling Layer-by-Layer Deposition and the Application for Durable Antifog Surfaces, *ACS App. Mat. & Inter.*, 8 (2016) 31951-31958.
48. J. Franklin, Z.Y. Wang, Refractive Index Matching: A General Method for Enhancing the Optical Clarity of a Hydrogel Matrix. Chem. Mat. 14 (2002) 4487-4489.
49. Labware chemical resistance table, ThermoFisher Scientific, https://tools.thermofisher.com/content/sfs/brochures/D20480.pdf (accessed 30.09.2017)
50. K. Norrman, A. Ghanbari-Siahkalia, N.B. Larsena, 6 Studies of spin-coated polymer films, Annu. Rep. Prog. Chem., Sect. C: Phys. Chem., 101 (2005) 174-201. Doi: 10.1039/B408857N.
51. A Zhiyuan Zeng, W.I. Liang, Y.H. Chu, H. Zheng, *In situ* TEM study of the Li–Au reaction in an electrochemical liquid cell. *Faraday Discuss.*, 176 (2014) 95-107.
52. R. Tran, E. Naseri, A. Kolasnikov, X. Bai, Y. Yang, A new generation of sodium chloride porogen for tissue engineering. Biotechnol. Appl. Biochem., 58 (2011) 335–344.
53. S. Bondza, E. Foy, J. Brooks, K. Andersson, J. Robinson, P. Richalet, J. Buijs, Real-time Characterization of Antibody Binding to Receptors on Living Immune Cells. Frontiers in Immunology, (2017), 8, 455 -. Doi: 10.3389/fimmu.2017.00455
54. V. Hlady, J. Buijs, H.P. Jennissen, Methods for Studying Protein Adsorption. Methods in Enzymology, 309 (2011), 402–429.
55. E.A. Vogler, Protein Adsorption in Three Dimensions. Biomaterials, 33 (2012) 1201–1237.
56. S. Lombardo S, S. Eyley, C Schütz, H. van Gorp, S. Rosenfeldt, G. Van den Mooter, W. Thielemans, Thermodynamic Study of the Interaction of Bovine Serum Albumin and Amino Acids with Cellulose Nanocrystals. Langmuir, 33 (2017), 5473-5481.

593 57. H. Orelma, I. Filpponen, L.S. Johansson, J. Laine, O.J. Rojas, Modification of Cellulose Films
594 by Adsorption of CMC and Chitosan for Controlled Attachment of Biomolecules,
595 Biomacromolecules, 12 (2011) 4311-4318.
596 58. N.H. Shah, E. Eryilmaz, E.D. Cowburn, T.W. Muir, Naturally Split Inteins Assemble through a
597 "Capture and Collapse" Mechanism. J. Am. Chem. Soc. 135 (2013) 18673-18681.
598 59. G. Vaaje-Kolstad, S.J. Horn, D.M.F. van Aalten, B. Synstad B, V.G.H. Eijsink, The Non-
599 catalytic Chitin-binding Protein CBP21 from Serratia marcescens Is Essential for Chitin
600 Degradation. *J. Biol. Chem.*, 280 (2005) 28492.
601 60. K. Manjeet, P. Purushotham, C. Neeraja, A.R. Podile, Bacterial chitin binding proteins show
602 differential substrate binding and synergy with chitinases, Microbiol. Res. 168 (2013) 461-468.
603 61. Z. Li, C. Li, K. Yang, L. Wang, C. Yin, Y. Gong, Y. Pang, Characterization of a chitin-binding
604 protein GP37 of Spodoptera litura multicapsid nucleopolyhedrovirus, Virus Res. 1-2 (2003)
605 113-122.
606 62. M. Hashimoto, T. Ikegami, O. Seino, N. Ohuchi, H. Fukada, J. Sugiyama, T. Watanabe,
607 Expression and Characterization of the Chitin-Binding Domain of Chitinase A1 from Bacillus
608 circulans WL-12. *J. of Bact.* 182 (2000) 3045–3054.
609 63. M. Hardt, R.A. Laine, Mutation of active site residues in the chitin-binding domain
610 ChBDChiA1 from chitinase A1 of Bacillus circulans alters substrate specificity: use of a green
611 fluorescent protein binding assay. *Arch. Biochem. & Biophys.*, 426 (2004) 286-297.
612 64. K. Somjit, K. Hara, M. Yoshimura, N. Matsuo, O. Kongpun, Y. Nozaki, Effect of shrimp chitin
613 and shrimp chitin hydrolysate on the state of water and dehydration-induced denaturation of
614 lizard fish myofibrillar protein. Food Sci. Technol. Res. J., 11 (2005) 106-11411.
615 65. P.S. Liu, H. Wang, X.M. Li, M.C. Rui, Z.H. Zeng, Localized surface plasmon resonance of Cu
616 nanoparticles by laser ablation liquid media. Rsc Advances, 5 (2015), 79738-79745.

66. M.K. Lee, T.G. Kim, W. Kim, Y.M. Sung, Surface plasmon resonance (SPR) electron and energy transfer in noble metal-zinc oxide composite nanocrystals. Journal of Physical Chemistry C, 112 (2008) 10079-10082.

67. M. Wysokowski, M. Motylenko, H. Stocker, V.V. Bazhenov, E. Langer, A. Dobrowolska, K. Czaczyk, R. Galli, A.L. Stelling, T. Behm, L. Klapiszewski, D. Ambrożewicz, M. Nowacka, S.L. Molodtsov, B. Abendroth, D.C. Meyer, K.J. Kurzydłowski, T. Jesionowski, H. Ehrlich, An extreme biomimetic approach: hydrothermal synthesis of beta-chitin/ZnO nanostructured composites. Journal of Materials Chemistry B, 1 (2013), 6469-6476.

**Tables**

Table 1. Surface properties of the SPR chips, before and after coating.

| Layer | Thickness [nm] | $n_r$ (670/785 nm) | Contact angle (at 1 sec/end)[1] [°] |
|---|---|---|---|
| Au (in air) | 50.88 | 0.2033/0.1978 | 20.7/21.2[2]<br>54.5/53.4[3] |
| Au-chitin (in air) | 1910 | 1.3908/1.3885 | 15.6/<1 |
| Au-chitin (in buffer) | 49.2<br>188.5 | 1.3617/1.3595<br>1.3463/1.3424 | <1/<1[4] |
| Au-PS (in air) | 10.7 | 1.6056/1.5971 | 49.9/48.5 |
| Au-PS-chitin(in air) | 1790 | 1.3678/1.3651 | 26.2°/<1 |
| AU-PS (in buffer) | 5.5 | 1.6056/1.5971 | N.D. |
| PS-Au-chitin (in buffer) | 26.4 | 1.3379/1.3350 | <1/<1[4] |

| | | |
|---|---|---|
| | 155.6 | 1.3357/1.3311 |

629 (1) Contact angle was determined over a range of 60 seconds; the first measured angle is at 1
630 second, while the end value is the average of a stable angle between 45 – 60 sec. Values lower than
631 1° represent a flat or absorbed water droplet on the surface; (2) Plasma cleaned Au surface; (3) Au
632 surface cleaned with $NH_3$ (30%)/$H_2O_2$ (30%)/$H_2O$ (1:1:5, v/v) oxidizing solution; (4) Chitin surface
633 was washed and dried under a nitrogen flow with buffer B.

634

635 Table 2. Kinetic binding properties to chitin and CBD-split intein.

| Protein | SPR Surface | $KD_1$ [nM] | $KD_2$ [nM] | $B_{max2}/B_{max1}$[1] |
|---|---|---|---|---|
| CBD-$IN_N$ | Au-Chitin | 76.3 | 0.0425 | 0.29 |
| CBD-$IN_N$ | Au-PS-Chitin | < 0.001[4] | 0.0052 | 0.08 |
| $IN_C$-eGFP | Au-Chitin + 0.025 nM[2] CBD-$IN_N$ | 90.3 | 0.0026 | 0.18 |
| $IN_C$-eGFP | Au-Chitin + 0.25 nM[3] CBD-$IN_N$ | 42.5 | < 0.001[4] | 0.23 |
| $IN_C$-eGFP | Au-PS-Chitin + 0.025[2] nM CBD-$IN_N$ | 13.8 | 0.0571 | 0.40 |
| $IN_C$-eGFP | Au-PS-Chitin + 0.25[3] nM CBD-$IN_N$ | 1.63 | 0.0509 | 0.48 |

636 (1) $B_{max2}/B_{max1}$ is the ratio of non-specific binding over specific binding; (2) 0.5 μg/ml; (3) 5 μg/ml;
637 (4) Upper limit for affinity, as precision in fits cannot be obtained due to the limited dissociation of
638 these samples.

639

640

641

642 Table 3. Selection of CBD and their binding characteristics with chitin.

| **Species** | **Domain name** | **Kd** | **Method** | **Ref** |
|---|---|---|---|---|
| *Serratia marcescens* | CBP21 | 1.4 μM | Solution depletion method | Vaaje-Kolstad *et al*. 2004 [59] |
| *Bacillus thuringiensis* serovar *kurstaki* | *Bt*CBD | 5.25 μM[1] (α-form) 3.46 μM (ß-form) | Solution depletion method | Manjeet *et al*. 2013 [60] |
| *B. licheniformis* DSM13 | *Bl*CBD | 5.98 μM[1] (α-form) 4.12 μM (ß-form) | Solution depletion method | Manjeet *et al*. 2013 [60] |
| *Spodoptera litura* multicapsid nucleopolyhedrovirus | GP37 | 0.061 μM | Solution depletion method | Li *et al*. 2003 [61] |
| *Bacillus circulans* | $CBD_{ChiA1}$ | N.D. ($K_r$ = 14.9 L/g) | Solution depletion method & ITC[3] | Hashimoto *et al*. 2000 [62] |
| *Bacillus circulans* | $CBD_{ChiA1}$ | 1.05 μM | Solution depletion method | Hardt and Laine 2004 [63] |
| *Bacillus circulans* | $CBD_{ChiA1}$ | 76.3 nM | SPR | *This study* |

| | | | | |
|---|---|---|---|---|
| | | | (Au-Chitin) | |
| *Bacillus circulans* | $CBD_{ChiA1}$ | < 0.001[4] | SPR (Au-PS-Chitin) | *This study* |

(1) $B_{max}$ values of *Bt*CBP were 2.18 ± 0.53 μmol/g for α-chitin and 2.92 ± 0.29 μmol/g for β-chitin;

(2) $B_{max}$ values of *Bli*CBP were 1.28 ± 0.007 μmol/g for α-chitin and 1.6 ± 0.18 μmol/g for β-chitin.

(3) $CBD_{CHA1}$ did not bind to soluble chitinous substrates, only specific binding to insoluble chitin was observed.

(4) Upper limit for affinity, as precision in fits cannot be obtained due to the limited dissociation of these samples.

Table 4. Optical parameters for the layers used in the Layersolver software for figure 4.

| **Sensor** | **Layer** | **d [nm]** | **$n_r$ (670 nm)** | **$n_r$ (785 nm)** | **k [RUI] (670 nm)** | **k [RIU] (785 nm)** | **Type** |
|---|---|---|---|---|---|---|---|
| Au | Prism | 0 | 1.5202 | 1.5162 | 0 | 0 | Standard |
| | Chromium | 2.25 | 1.40148 | 2.11206 | 2.36163 | 1.40291 | Standard |
| | Gold | 50.88 | 0.20332 | 0.19791 | 3.384549 | 4.89071 | Standard |
| | Air | 0 | 1 | 1 | 0 | 0 | Standard |
| Au-Chitin | Prism | 0 | 1.5202 | 1.5162 | 0 | 0 | Standard |
| | Chromium | 3.37 | 3.5889 | 1.9545 | 1.44746 | 8.01544 | Standard |
| | Gold | 46.3 | 0.22395 | 0.26372 | 3.89604 | 4.90096 | Standard |
| | Chitin | 1910 | 1.39075 | 1.38845 | 0 | 0 | Standard |
| | Air | 0 | 1 | 1 | 0 | 0 | Standard |
| Au-Chitin (lower limit) | Prism | 0 | 1.5202 | 1.5162 | 0 | 0 | Standard |
| | Chromium | 3.18 | 1.6162 | 2.49777 | 2.27739 | 2.17001 | Standard |

| | | | | | | | |
|---|---|---|---|---|---|---|---|
| | Gold | 49.41 | 0.20042 | 0.20038 | 3.95704 | 5.03863 | Standard |
| | Chitin | 49.42 | 1.36168 | 1.36168 | -0.019 | -0.019 | Standard |
| | Buffer | 0 | 1.3342 | 1.332 | 0 | 0 | Standard |
| Au-Chitin (upper limit) | Prism | 0 | 1.5202 | 1.5162 | 0 | 0 | Standard |
| | Chromium | 3.18 | 1.6162 | 2.49777 | 2.27739 | 2.17001 | Standard |
| | Chitin | 49.41 | 0.20042 | 0.20038 | 3.95704 | 5.03863 | Standard |
| | Gold | 188.51 | 1.34628 | 1.3428 | -0.034 | -0.034 | Standard |
| | Buffer | 0 | 1.3342 | 1.332 | 0 | 0 | Standard |
| Au-PS | Prism | 0 | 1.5202 | 1.5162 | 0 | 0 | Standard |
| | Chromium | 1.75 | 1.66531 | 2.49949 | 5.13164 | 7.85818 | Standard |
| | Gold | 49.75 | 0.20195 | 0.1418 | 3.55135 | 4.47549 | Standard |
| | Polystyrene | 10.89 | 1.6 | 1.6 | -0.06 | -0.06 | Linear |
| | Air | 0 | 1.0003 | 1.003 | 0 | 0 | Standard |
| Au-PS Chitin | Prism | 0 | 1.5202 | 1.5162 | 0 | 0 | Standard |
| | Chromium | 1.09 | 4.5166 | 0.29287 | -0.06537 | 1.7632 | Standard |
| | Gold | 50.88 | 0.2391 | 0.27063 | 4.08143 | 5.02307 | Standard |
| | Polystyrene | 5.5 | 1.6056 | 1.5987 | 0 | 0 | Standard |
| | Chitin | 1790 | 1.3678 | 1.3651 | 0 | 0 | Standard |
| | Air | 0 | 1.0003 | 1.0003 | 0 | 0 | Standard |
| Au-PS-Chitin (lower limit) | Prism | 0 | 1.5202 | 1.5162 | 0 | 0 | Standard |
| | Chromium | 0.19 | -3.45785 | 0.57461 | -6.98458 | 0.10471 | Standard |
| | Gold | 50.22 | 0.25187 | 0.26315 | 4.04329 | 5.03546 | Standard |

| | | | | | | | |
|---|---|---|---|---|---|---|---|
| | Polystyrene | 5.5 | 1.6056 | 1.5987 | 0 | 0 | Standard |
| | Chitin | 27.25 | 1.33795 | 1.33795 | -0.027 | -0.027 | Standard |
| | Buffer | 0 | 1.3342 | 1.332 | 0 | 0 | Standard |
| Au-PS-Chitin (upper limit) | Prism | 0 | 1.5202 | 1.5162 | 0 | 0 | Standard |
| | Chromium | -0.22 | 6.18797 | -4.27058 | -3.45867 | 4.7062 | Standard |
| | Gold | 50.41 | 0.25157 | 0.25931 | 4.05202 | 4.99513 | Standard |
| | Polystyrene | 5.5 | 1.6056 | 1.5987 | 0 | 0 | Standard |
| | Chitin | 154.6 | 1.33574 | 1.33574 | -0.04 | -0.04 | Standard |
| | Buffer | 0 | 1.3342 | 1.332 | 0 | 0 | Standard |

**Figures**

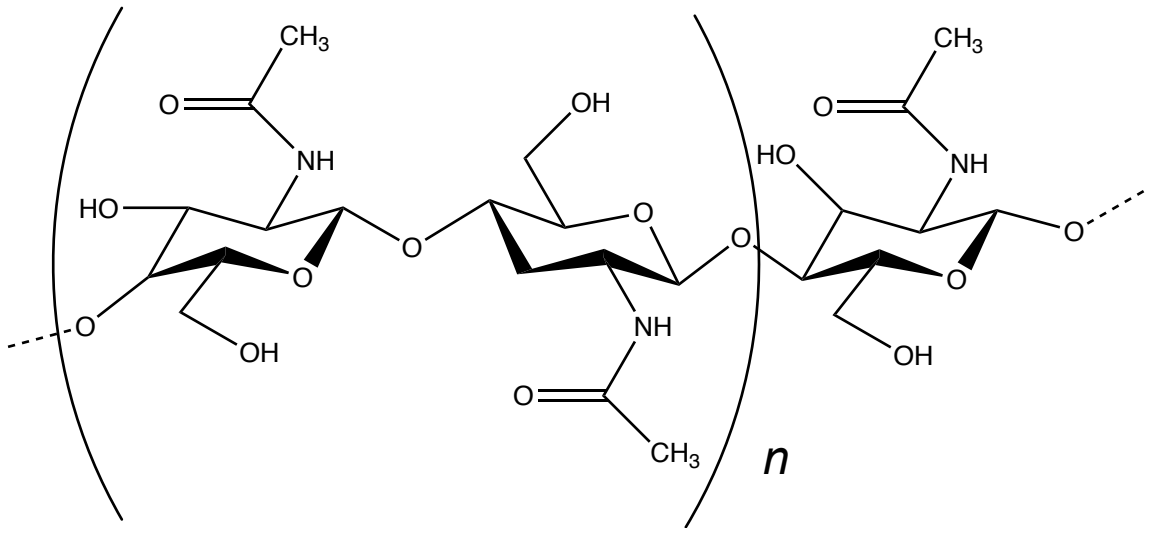


**Figure 1.** Chemical structure of chitin. Chitin polymers derived from shrimp shell have a typical degree of polymerization of 493 – 605 [64].

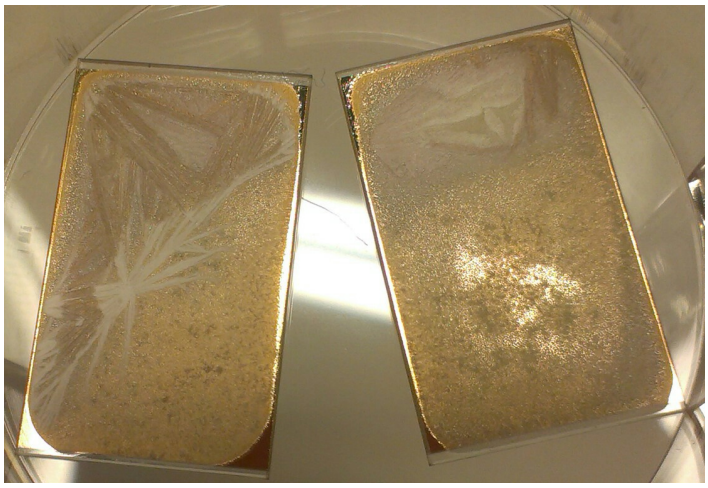

**Figure 2.** Au leaching of SPR chips due to LiCl in the 0.1% chitin DMA/5% LiCl solution. White areas are void of gold.

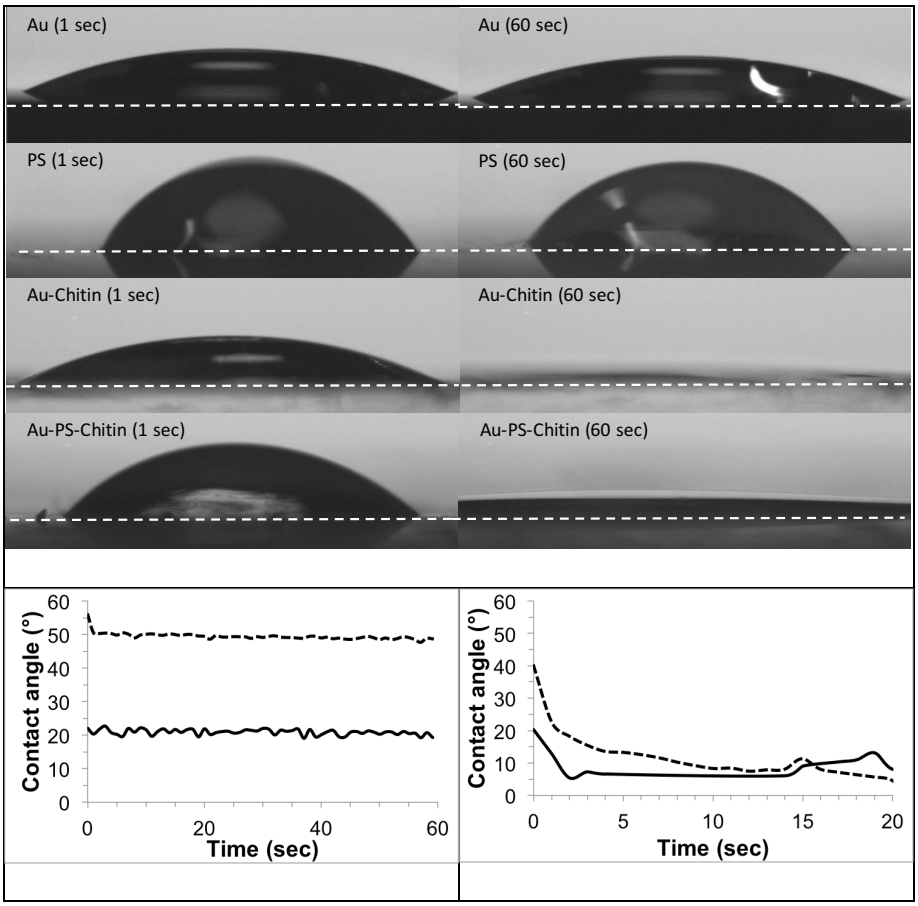


**Figure 3.** Water droplet behavior during contact angel measurements. The white dashed line in the upper panels depicts the droplet-surface interface. Droplets on Au (solid line) or Au-PS (dashed

line) were stabile (bottom left), the droplet on dry Au-Chitin surface (solid line) reached a contact angle below 10° after 2 seconds, while the droplet on the dry Au-PS-Chitin surface (dashed line) reached a contact angle below 10° after 20 seconds (bottom right). All surfaces depicted here were plasma cleaned prior to measurements or spin-coating.

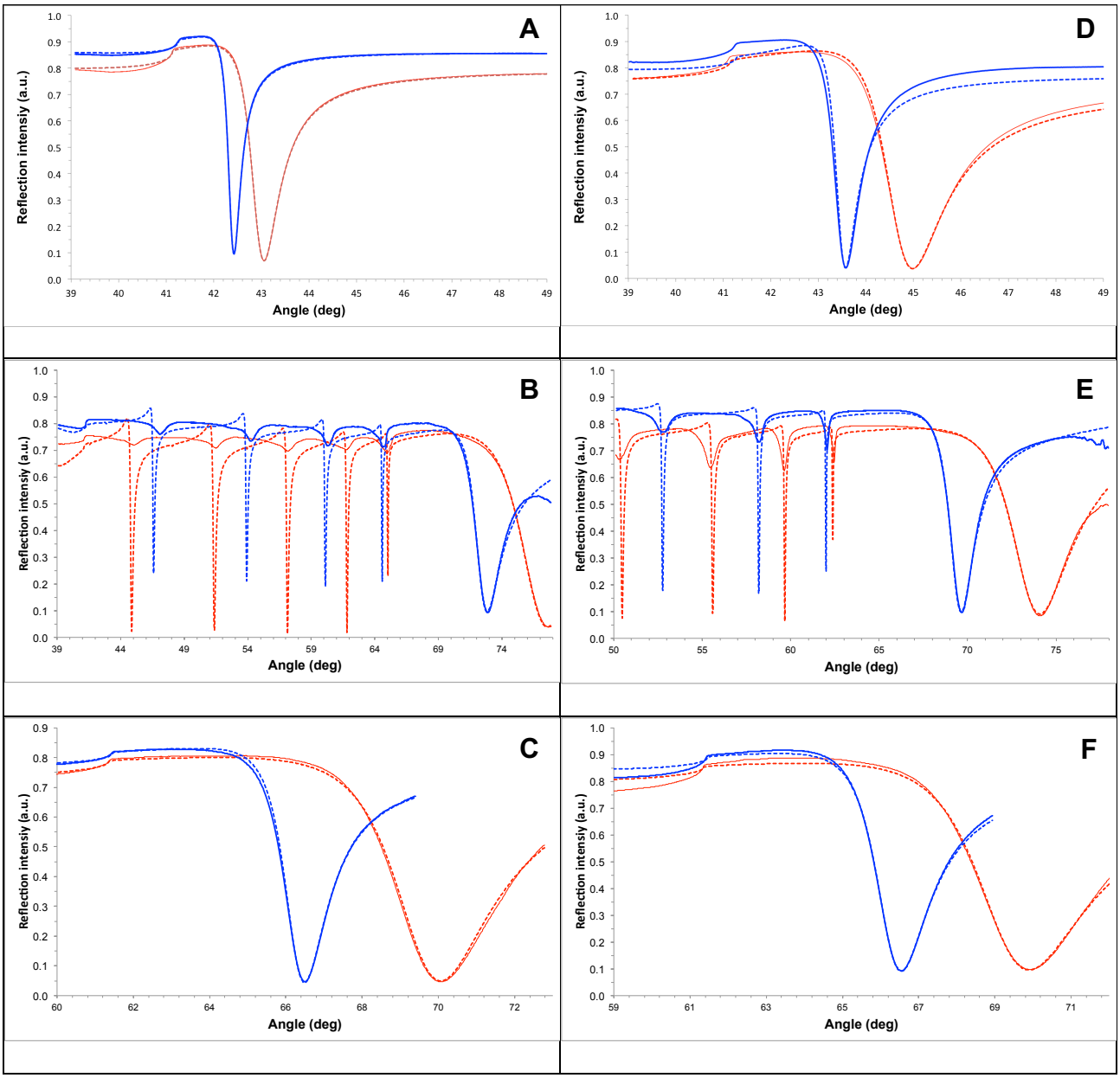


**Figure 4.** SPR full angle scans of (A) pure SPR sensor background, (B) spin-coated chitin on Au, (D) PS on Au, and (E) spin-coated chitin on PS on Au; 670 nm: red solid line, 785 nm: blue solid

line with corresponding Layer solver fits (dashed lines). The optical parameters used for the Layer solver fitting are listed in table 4.

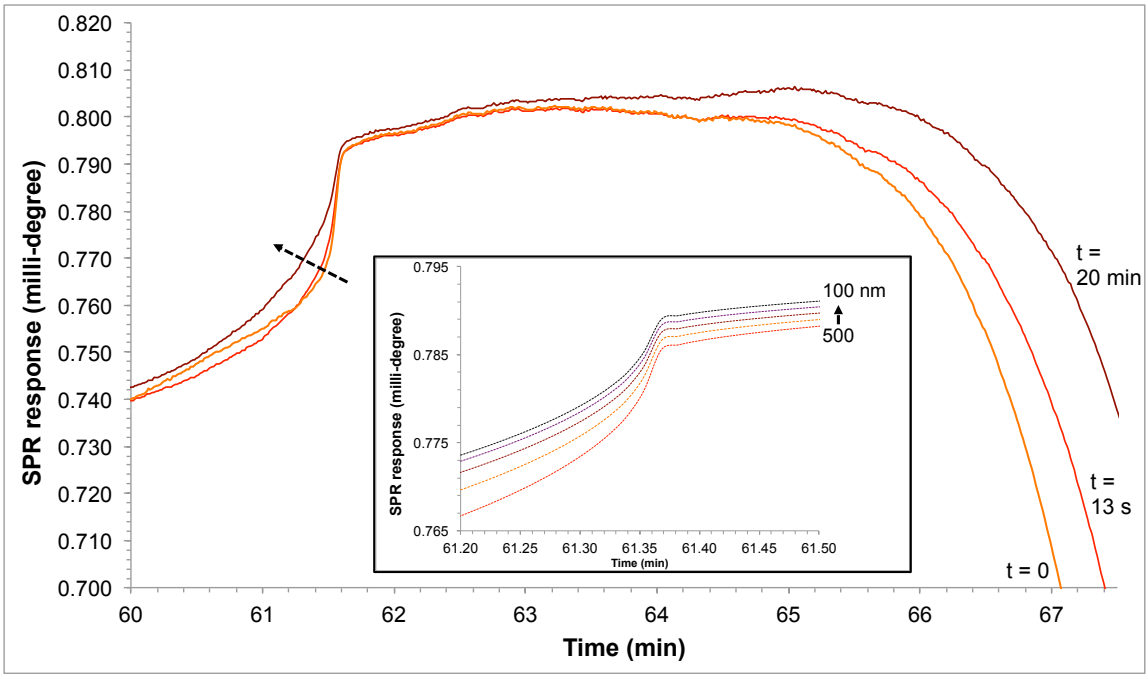


**Figure 5.** TIR detail of the full angle scans of spin-coated chitin on Au. For clarity the data derived from 670 nm is depicted, however the models were fitted for 670 and 785 nm simultaneously. In orange (t = 0) is the first time point after buffer B is introduced, in dark red (t = 20) the base line in the SPR sensorgram is stable. The dashed arrow indicates the shift of the shape of the TIR angle from thicker to a thinner layer. Inset: Layersolver model of the change of the TIR angle shape from 500 nm to 100 nm (chitin on Au).

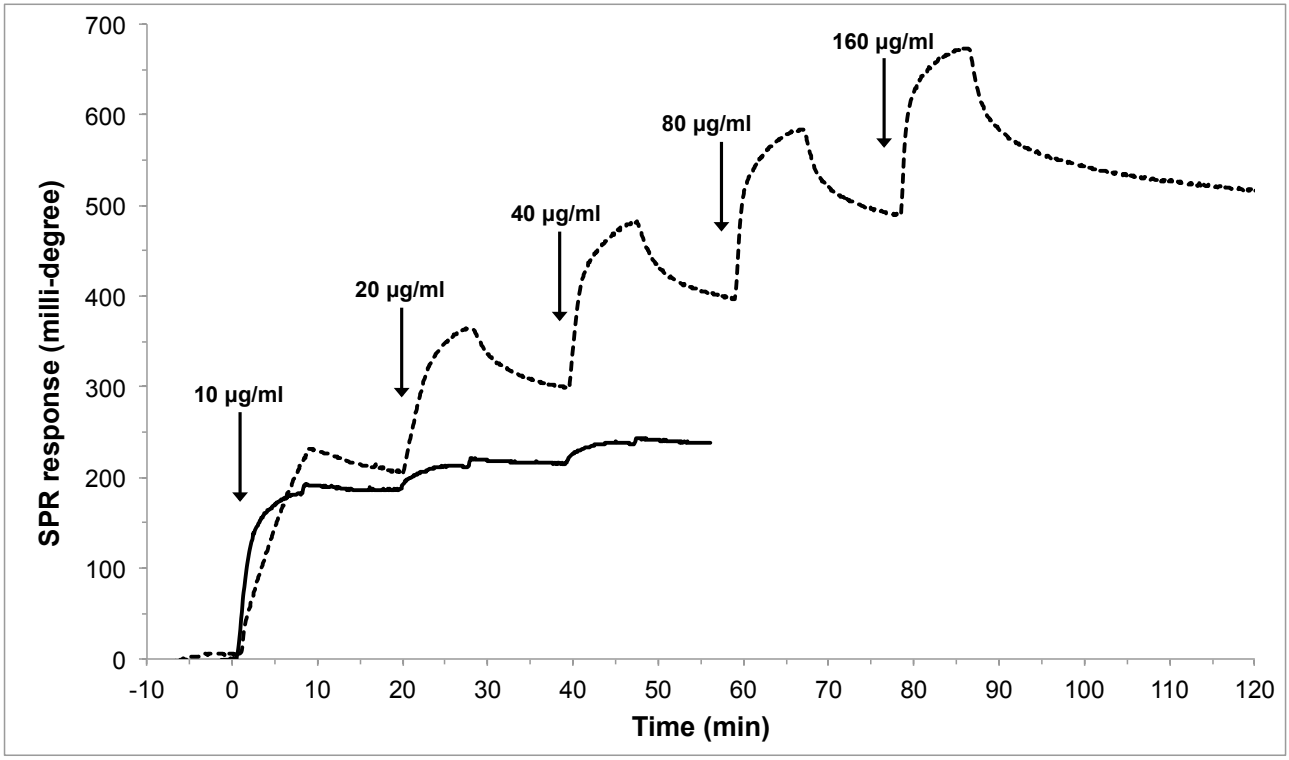


**Figure 6.** Titration of CBD-$IN_N$ onto a spin-coated (SC) chitin layer on Au (dashed) or SC chitin layer on PS (solid line). Concentrations are equivalent to 490, 981, 1961, 3922, and 7854 nM.

689

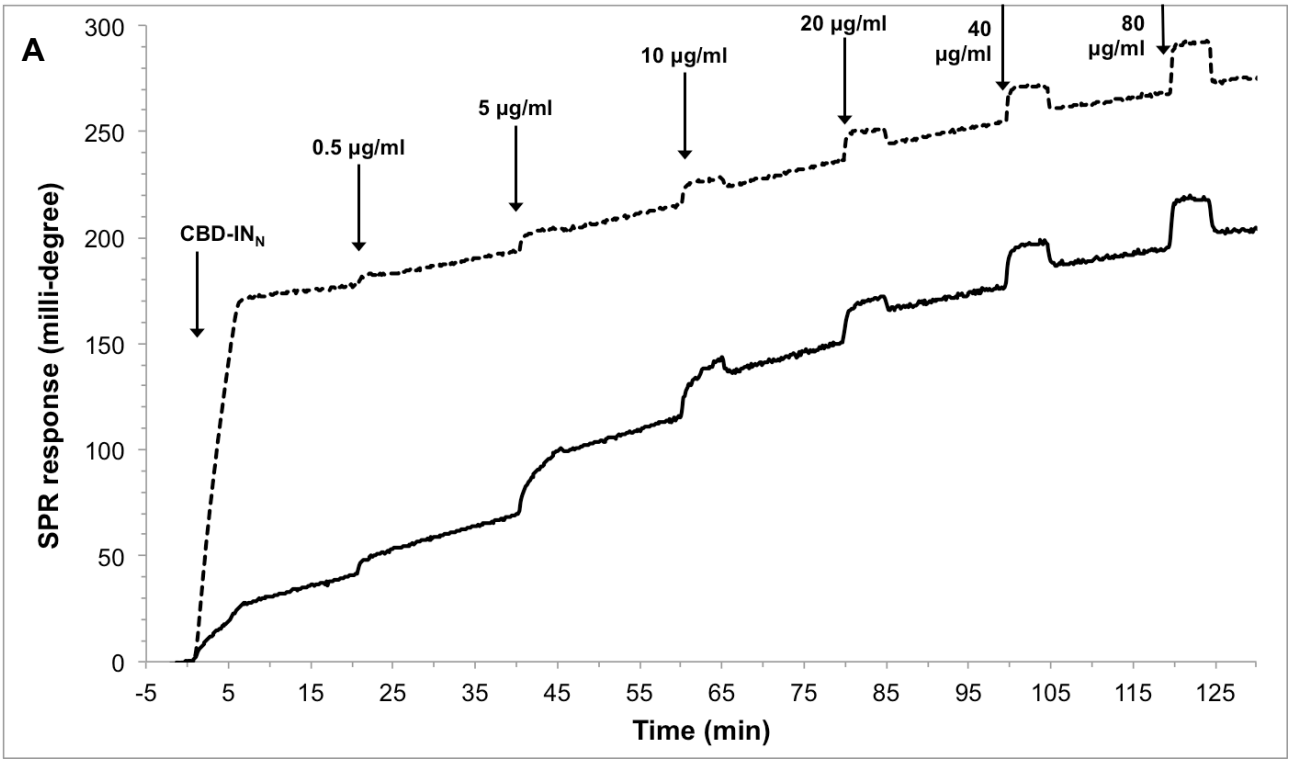


690

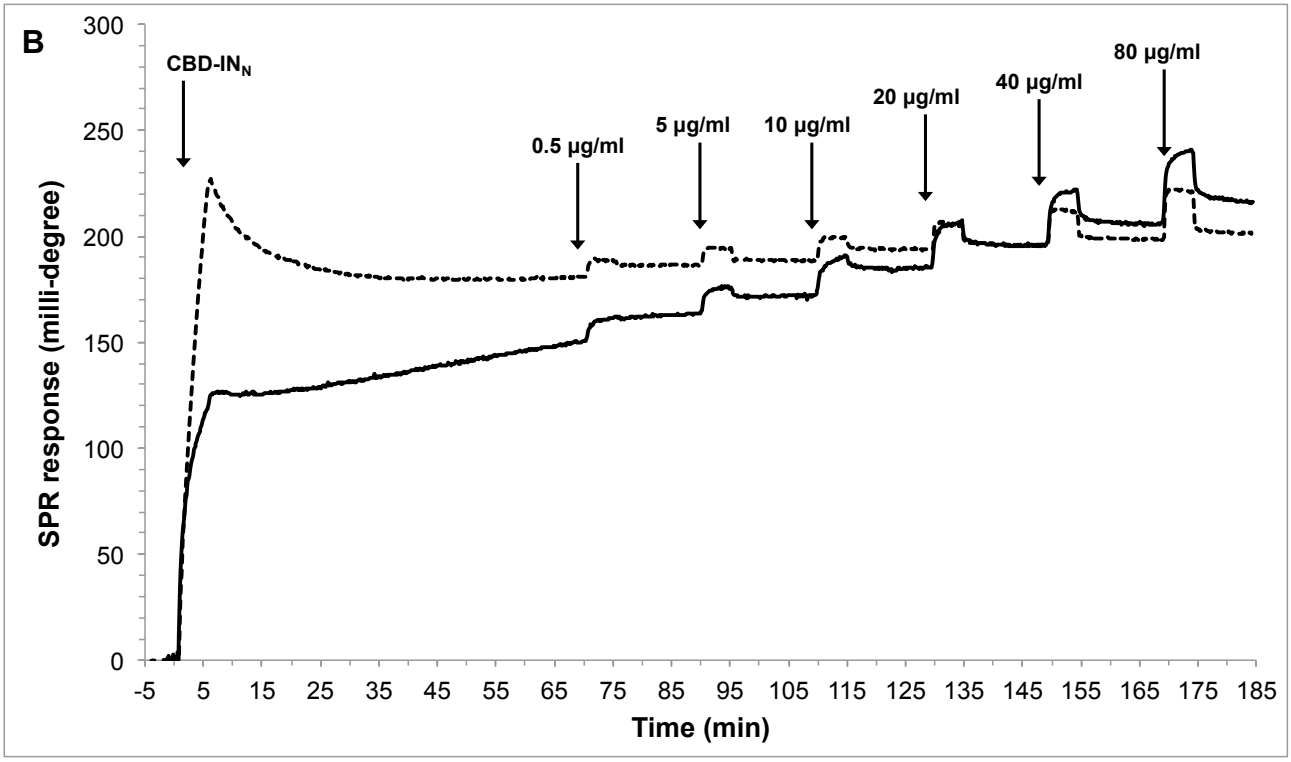


691

692 **Figure 7.** Titration of $IN_C$-eGFP onto a spin-coated chitin layer on (A) Au or (B) SC chitin layer on

693 PS after binding of 5 µg/ml CBD-$IN_N$ (dashed lines) or 0.5 µg/ml CBD-$IN_N$ (solid lines).

694 Concentrations are equivalent to 17.5, 175, 350, 701, 1401, 2803 nM.

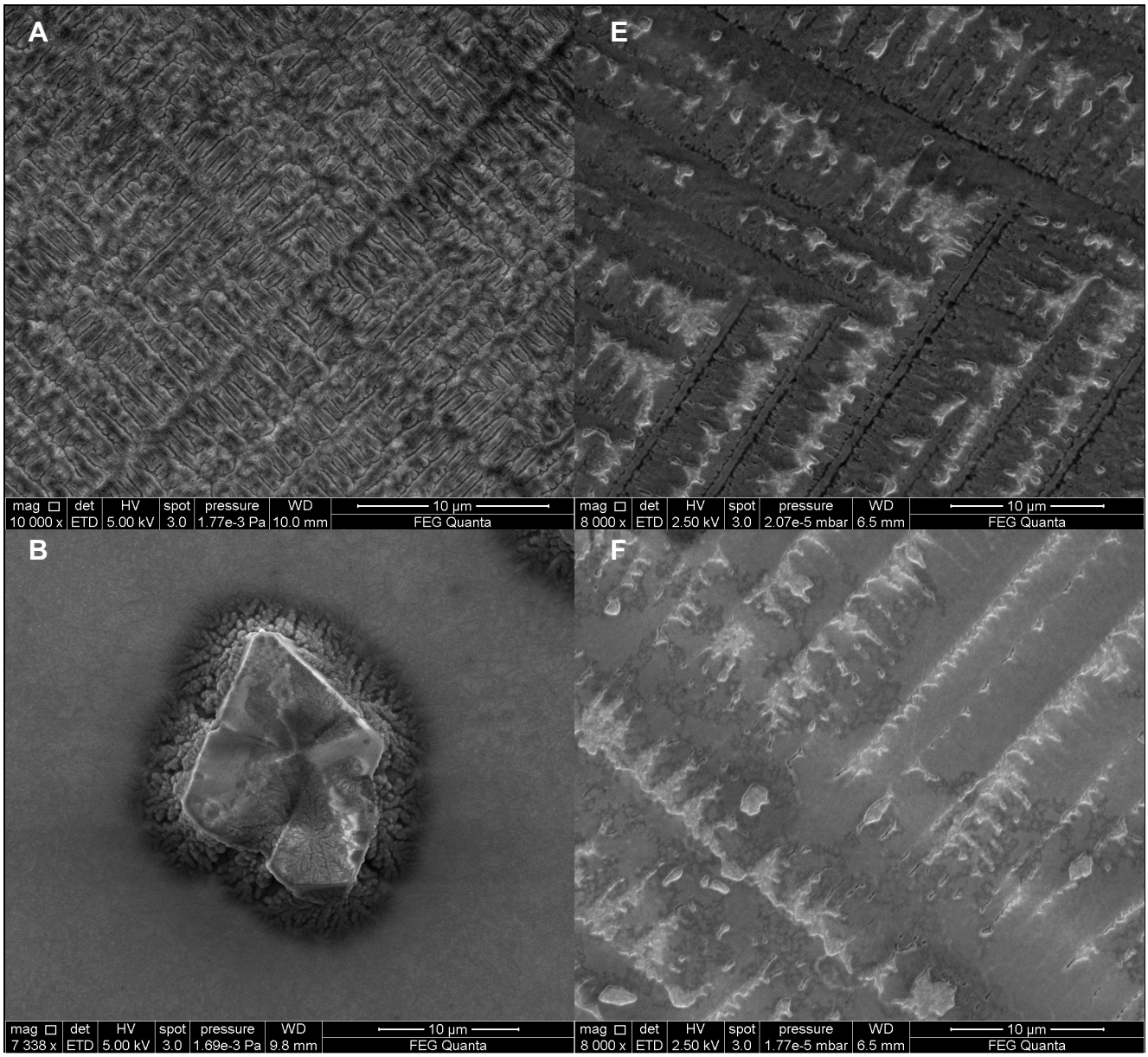
A
mag det HV spot pressure WD 10 µm
10 000 x ETD 5.00 kV 3.0 1.77e-3 Pa 10.0 mm FEG Quanta
E
mag det HV spot pressure WD 10 µm
8 000 x ETD 2.50 kV 3.0 2.07e-5 mbar 6.5 mm FEG Quanta
B
mag det HV spot pressure WD 10 µm
7 338 x ETD 5.00 kV 3.0 1.69e-3 Pa 9.8 mm FEG Quanta
F
mag det HV spot pressure WD 10 µm
8 000 x ETD 2.50 kV 3.0 1.77e-5 mbar 6.5 mm FEG Quanta

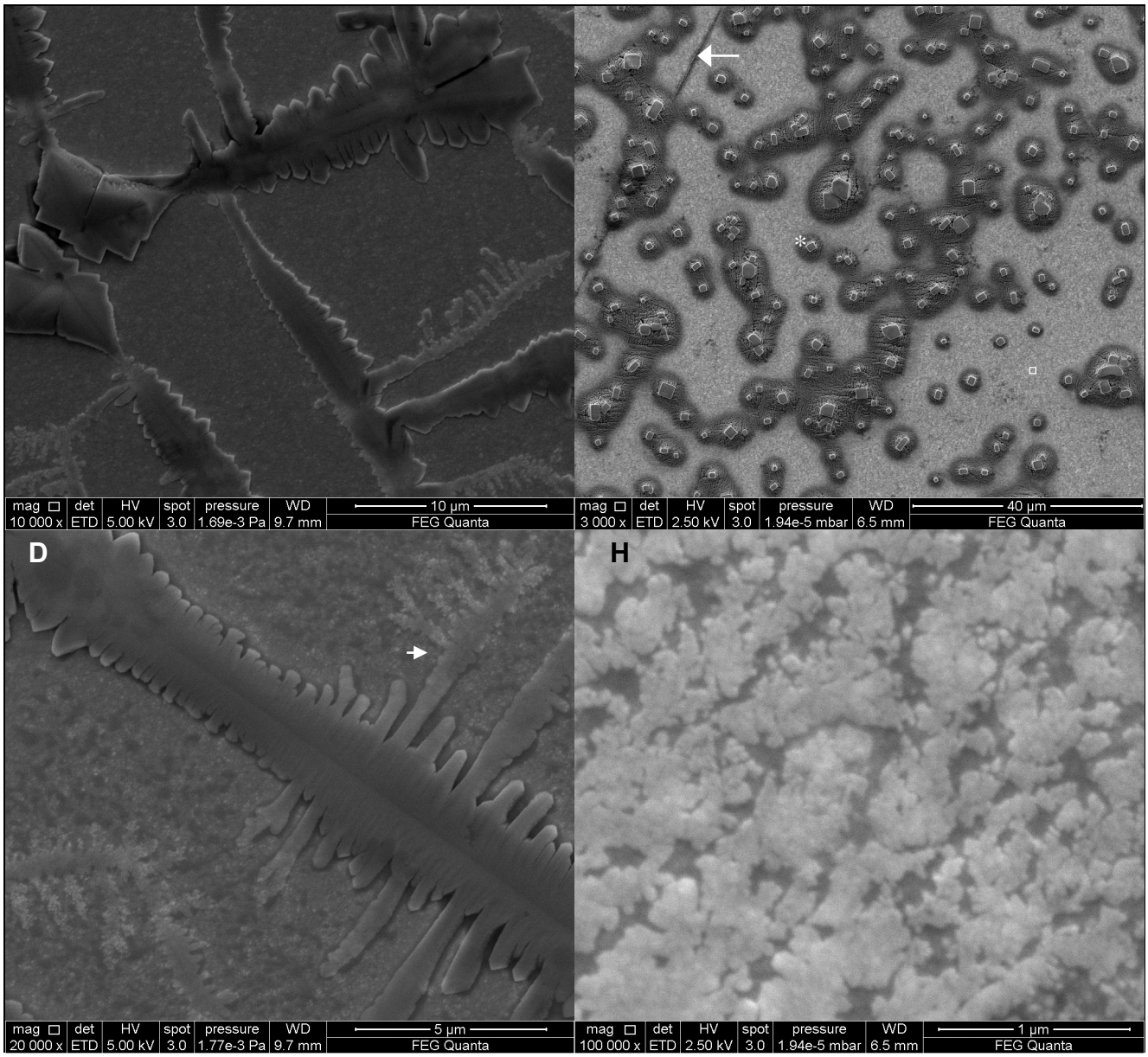


**Figure 8.** SEM images of the chitin surface (A) on Au in air (after 5 min), (B) on Au in air (after 1 hour), (C) on Au after 15 min of buffer B in the SPR flow cell (at 20 µL/min), and (D) as C, with higher resolution (arrow shows microstructure of chitin is attached to the macrostructure). (E) on Au-PS in air (5 min), (F) on PS in air (after 1 hour), (G) on Au-PS after 15 min of buffer B (at 20 µL/min); (*) cubic shapes are likely sodium chloride crystals; the arrow in F shows a line of non-coated Au, between two areas of PS coating; small white square in F the magnified area shown in G, and (H) as G, with higher resolution.

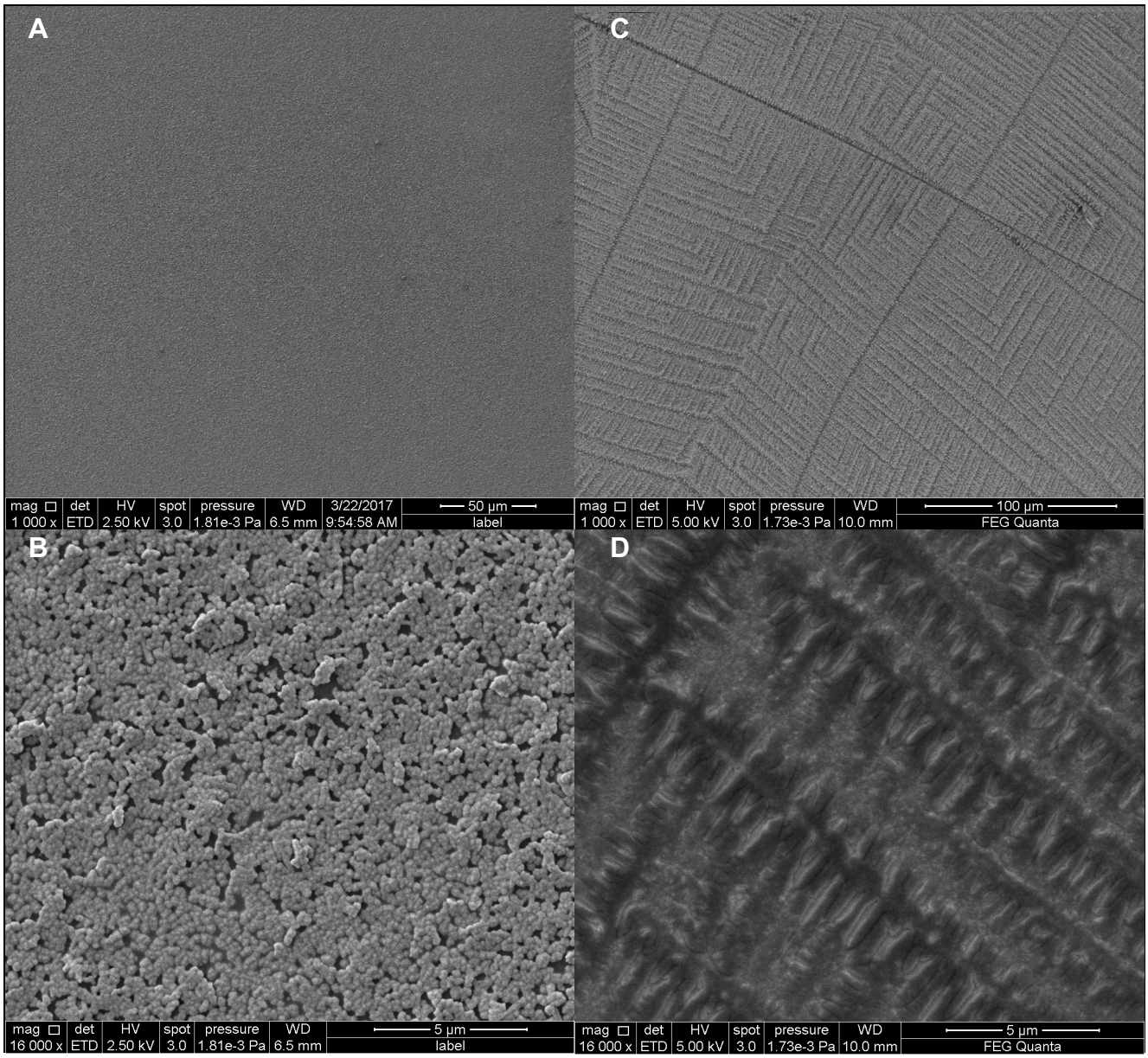


**Figure 9.** SEM images of chitin spin coated on Au-PS in air, after (A) < 30 seconds, (B) < 30 seconds at higher magnification, (C) 5 minutes, (D) 5 minutes at higher magnification.